Research on Chemical Intermediates (2020) 46:3277–3294
https://doi.org/10.1007/s11164-020-04130-x

Preparation and characterization of a novel organic–inorganic hybrid nanostructure: application in synthesis of spirocompounds

Najmieh Ahadi[1] · Mohammad Ali Bodaghifard[1,2] · Akbar Mobinikhaledi[1]

Received: 15 December 2019 / Accepted: 16 March 2020 / Published online: 4 May 2020

Abstract

Immobilization and heterogenization of acidic/basic groups or organic tags on inorganic supports have found many important applications in recent years. In this investigation, a new hybrid organic–inorganic nanostructure was prepared. The structure of novel nanomaterial was characterized by Fourier transform infrared spectroscopy, X-ray diffraction, thermogravimetric analysis, vibrating sample magnetometer, scanning electron microscopy and the energy-dispersive X-ray spectroscopy techniques. The spirocompounds, especially spiroperimidines and pyranopyrazoles, are important structures with diverse biological activities and many applications in industries. So, the prepared hybrid nanomaterial was used as an efficient catalyst in the one-pot, green and simple protocol for the synthesis of pyranopyrazole, spiropyranopyrazole and spiroperimidine derivatives. The structure of some compounds is characterized by FT-IR, ^{1}H-NMR and ^{13}C-NMR analyses. In addition, the proposed intermediates were synthesized and identified to prove the presented mechanism of the reaction. This hybrid nanomaterial is a recyclable and highly efficient heterogeneous catalyst and easily separated by an external magnet from the reaction media. The short reaction time, high efficiency, operational safety and use of environmentally benign solvent are some benefits of this procedure.

Electronic supplementary material The online version of this article (https://doi.org/10.1007/s11164-020-04130-x) contains supplementary material, which is available to authorized users.

✉ Mohammad Ali Bodaghifard
mbodaghi2007@yahoo.com; m-bodaghifard@araku.ac.ir

[1] Department of Chemistry, Faculty of Science, Arak University, 38156-8-8349 Arāk, Iran

[2] Institute of Nanosciences and Nanotechnology, Arak University, 38156-88349 Arāk, Iran

Graphic abstract

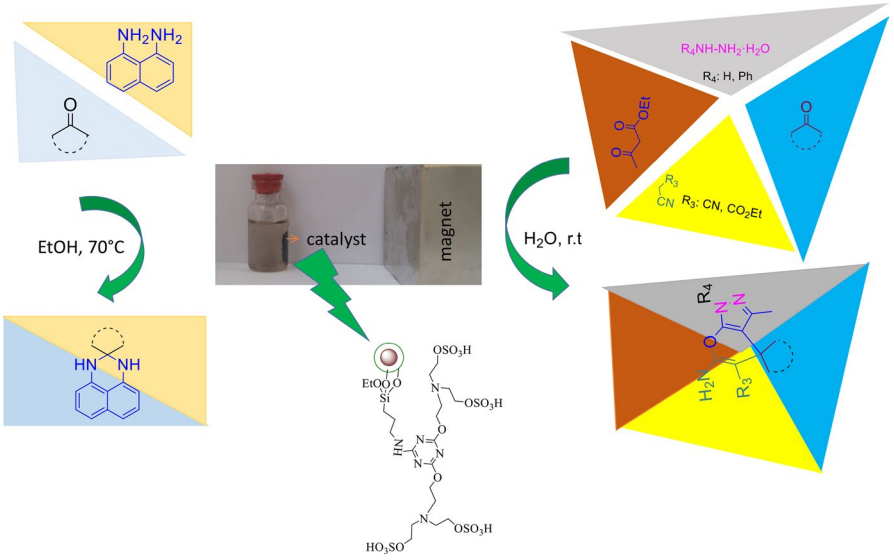

Keywords Nanostructures · Hybrid materials · Heterogeneous catalysis · Pyranopyrazole · Spirocompounds · Green chemistry

Introduction

Magnetic nanoparticles have found many applications in various fields such as drug delivery, hyperthermia, magnetic resonance imaging (MRI), cell and stem cell separation, pharmacology, enzyme immobilization, magnetic fluids, sensor, pigments and catalysis area [1–4]. In recent years, magnetic nanoparticles have received considerable attention as the catalysts in organic chemistry because of exceptional properties including high surface area, thermal stability, low toxicity, strong activity, easy separation (by a magnet), the capability of surface modification, reusability and recyclability in the organic reaction for several runs without noticeable loss of catalytic activity [4–10]. The manganese ferrite ($MnFe_2O_4$), as a class of soft magnetic materials with distinct advantages like extraordinary saturation, low toxicity, excellent compatibility and superparamagnetic properties, has obtained particular interest [11].

Multicomponent reactions (MCRs) have attracted considerable attention in medicinal chemistry and modern organic synthesis because of time, energy and environmental conservation [12]. MCRs produce complex and diverse combinations of products and follow many principles of green chemistry, such as solvent-free or aqueous condition, atom economy, energy saving with short reaction times, waste diminish, high yields and selectivity [12–14]. Possible elimination of hazardous solvents and using

solvent-free or aqueous conditions in MCRs have a notable impact on the protection of the environment [12–14].

Among the various classes of heterocyclic compounds, perimidines and pyranopyrazoles are important structures with diverse biological activities [15–19]. Furthermore, perimidine and pyranopyrazole derivatives have many applications in industries and agriculture, such as organic solar cells, plasma display panels, optical recording media, molecular switches, photochemical memory devices, insecticides, acaricides and herbicides [17, 20]. Spirocompounds with structural rigidity are bioactive materials like antimicrobial, hypoglycemic, antifungal, anti-inflammatory, anti-bacterial and anticancer [16, 21–25]. Due to their broad range of pharmacological activity and industrial applications, several methods have been reported for the synthesis of pyranopyrazole, spiropyranopyrazoles, spiroperimidines and other spirocompounds [26–29]. However, most of these methods experience limitations such as low yields, elevated temperatures, prolonged reaction time and unrecyclable catalysts. As a result, the development of green and straightforward methods for the synthesis of pyranopyrazole, spiropyranopyrazoles and spiroperimidines is necessary.

The heterogenization of homogeneous acidic and basic groups in catalytic reactions (such as covalently bound acidic or basic catalysts) typically allows for the easy separation and beneficial reuse of catalysts. The inorganic-supported catalysts, especially hybrid organic–inorganic magnetic nanomaterials, have been widely used in recent years that could be extremely useful in the catalysis area [6]. Hence, herein, we introduce a clean and efficient synthetic way for the preparation of pyranopyrazole, spiropyranopyrazoles and spiroperimidines gently using MNPs@SiO_2-BTEAT-SO_3H particles as a novel hybrid catalyst in mild and green conditions.

Results and discussion

Preparation of MNPs@SiO_2-BTEAT-SO_3H catalyst

The schematic preparation of MNPs@SiO_2-BTEAT-SO_3H particles is shown in Scheme 1. $MnFe_2O_4$ nanoparticles were prepared using the co-precipitation method [30]. Subsequently $MnFe_2O_4$ nanoparticles were coated with a silica layer via the Stöber procedure [30, 31]. Then, 3-aminopropyltriethoxysilane (APTS) was bound covalently to the OH groups on the $MnFe_2O_4$@SiO_2 surface to gain $MnFe_2O_4$@SiO_2-$PrNH_2$ nanostructure. $MnFe_2O_4$@SiO_2-$PrNH_2$ nanoparticles in the presence of Et_3N as a base were reacted with cyanuric chloride. $MnFe_2O_4$@SiO_2-Pr-BTEAT particles were prepared from the reaction between $MnFe_2O_4$@SiO_2-Pr-$TDCl_2$ and triethanolamine. Ultimately, the reaction of $MnFe_2O_4$@SiO_2-Pr-BTEAT with chlorosulfonic acid was performed, and the desired hybrid material (MNPs@SiO_2-BTEAT-SO_3H) was obtained.

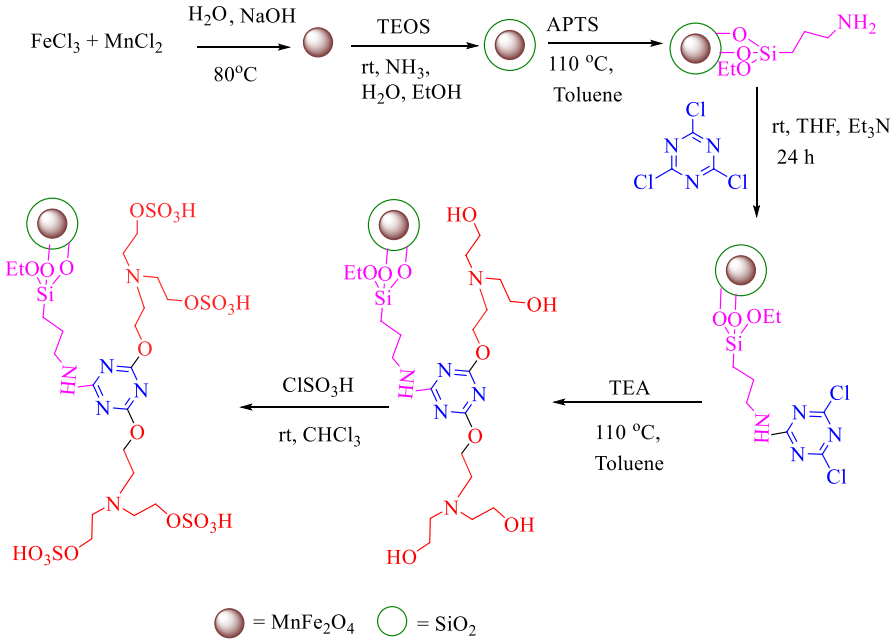

Scheme 1 Preparation steps of MNPs@SiO_2-BTEAT-SO_3H as a new hybrid catalyst

Characterization of MNPs@SiO_2-BTEAT-SO_3H catalyst

The FT-IR spectroscopy

For all synthesized MNPs (Fig. 1), the characteristic band at 587 cm^{-1} is properly assigned to the Fe–O bond stretching vibration. Also, the H–O–H twisting vibration appeared at 1627 cm^{-1}. The absorption bands at 459 cm^{-1} (rocking mode), 800 and 954 cm^{-1} (bending), and 1087 cm^{-1} (asymmetric stretching) are related to Si–O–Si groups and confirm the formation of SiO_2 shell (Fig. 1b). The weak bands at 2974 and 2930 cm^{-1} are attributed to C–H stretching vibrations, establishing the covalent bonding of organic tags. The spectra of MNPs-$TDCl_2$ and MNPs-BTEAT (Fig. 1d, e) show bands around 1450 to 1650 cm^{-1} that are typically corresponding to C=N, C=C, C–N and C–O bonds and confirm the heterocyclic ring attachment [27]. The appeared band around 700 cm^{-1} at the spectrum of MNPs-$TDCl_2$ (Fig. 1d) is related to C–Cl stretching vibration. The elimination of this band in the spectrum of MNPs-BTEAT (Fig. 1e) promptly confirms the successful substitution of Cl groups with triethanolamine. Eventually, MNPs@SiO_2-BTEAT-SO_3H was characterized by the absorption band at 1201 cm^{-1}, related to O=S=O moieties, that has overlapped with Si–O–Si stretching band [32] (Fig. 1f).

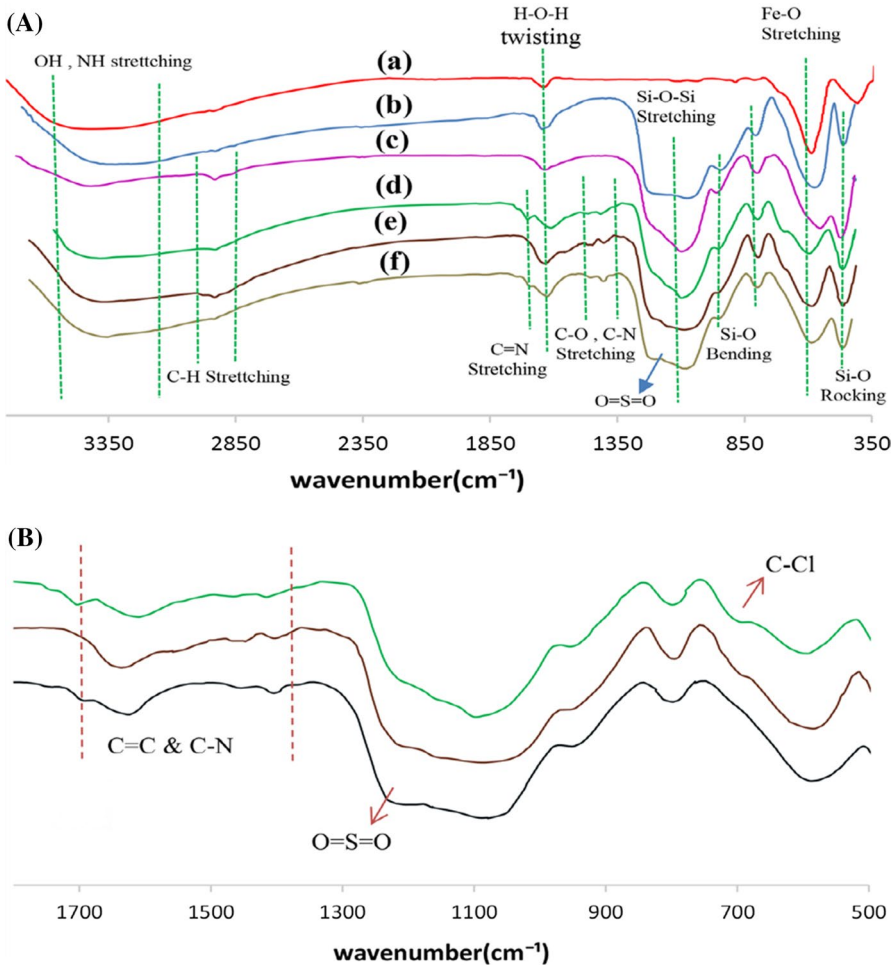

Fig. 1 **A** FT-IR spectra for **a** $MnFe_2O_4$, **b** $MnFe_2O_4$@SiO_2, **c** $MnFe_2O_4$@SiO_2-$PrNH_2$, **d** $MnFe_2O_4$@SiO_2-Pr-$TDCl_2$, **e** $MnFe_2O_4$@SiO_2-Pr-BTEAT, **f** MNPs@SiO_2-BTEAT-SO_3H. **B** Expanded FT-IR spectra for (**d**, **e**, **f**)

The XRD diffraction patterns

The XRD patterns for $MnFe_2O_4$ (a) and MNPs@SiO_2-BTEAT-SO_3H (b) are shown in Fig. 2. Diffraction peaks at $2\theta = 30$, 35, 43, 53, 57 and 63 can be assigned to the (200), (311), (400), (331), (422) and (333) miller planes of $MnFe_2O_4$, respectively. These data are granting to the standard $MnFe_2O_4$ sample (JCPDS card no. 1964-73) and instantly confirm the cubic spinel structure for $MnFe_2O_4$ nanoparticles. The broad peak at $2\theta = 17$–25 is related to the amorphous SiO_2 shell on the surface of $MnFe_2O_4$ cores (Fig. 2b) [4]. The average size for MNPs@SiO_2-BTEAT-SO_3H is calculated to be about 29 nm [25].

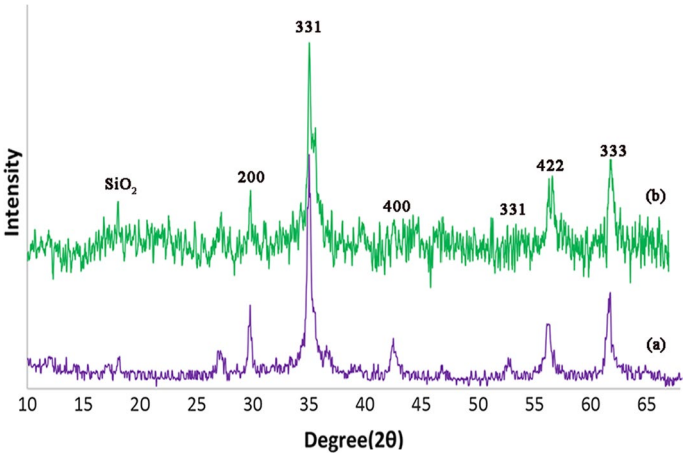

Fig. 2 XRD patterns for $MnFe_2O_4$ (**a**) and MNPs@SiO_2-BTEAT-SO_3H (**b**)

The TGA-DTA and DTG analyses

The stability and functionalization of the MNPs@SiO_2-BTEAT-SO_3H catalyst were evaluated by the TGA, DTG and DTA analyses (Fig. 3). TGA curve outlined three steps of weight loss for the MNPs@SiO_2-BTEAT-SO_3H catalyst at 25–800 °C. The first step shows 3% weight loss at $T < 200$ °C that is related to the removal of physically absorbed solvent and surface hydroxyl groups. The second step shows 12%

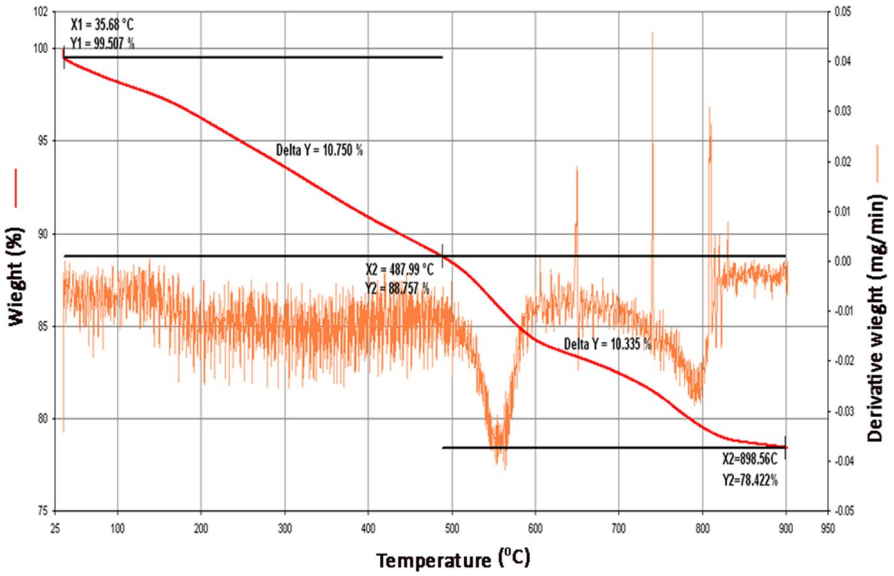

Fig. 3 TGA and DTG analysis for MNPs@SiO_2-BTEAT-SO_3H

weight loss at 200–590 °C range, attributed to the decomposition of organic moieties in the hybrid nanomaterial. The weight loss (11%) at $T > 600$ °C shows the destruction of the silica layer and particle deformation. This mass loss shows that 0.13 mmol of H^+ was loaded on 1 gr MNPs@SiO_2-BTEAT-SO_3H catalyst. These results assure the stability of the MNPs@SiO_2-BTEAT-SO_3H particles at below 200 °C that is in agreement with back titration results and establish that the organic groups are successfully loaded on the surface of $MnFe_2O_4$ nanoparticles. DTG analysis shows that MNPs@SiO_2-BTEAT-SO_3H nanoparticles were deformed at 580 °C. Moreover, the DTA diagram (blue curve) revealed that this gradual process was endothermic.

Magnetic properties (VSM analysis)

The magnetization curve of $MnFe_2O_4$ and MNPs@SiO_2-BTEAT-SO_3H is shown in Fig. 4. The magnetization hysteresis loops for samples (a) and (b) are S-like and show superparamagnetic properties for them. The saturation magnetization (Ms) is 33 Oe for $MnFe_2O_4$ (a) and 22 Oe for MNPs@SiO_2-BTEAT-SO_3H (b). Data show that Ms for MNPs@SiO_2-BTEAT-SO_3H is lower than the $MnFe_2O_4$ core. These direct results can amply confirm the successful preparation of MNPs@SiO_2-BTEAT-SO_3H structure.

The SEM, EDS and EDS map scan analyses

The size and morphology of MNPs@SiO_2-BTEAT-SO_3H particles were considered employing the FE-SEM analysis (Fig. 5a). The results show an average diameter of 20–35 nm and nearly spherical shape of nanoparticles that are in agreement with the obtained results from XRD patterns. The energy-dispersive X-ray spectroscopy (EDS) result, obtained from FE-SEM analysis, is shown in Fig. 5b. This analysis indicates clearly the presence of S, N, O, Si, Fe and Mn elements. The higher intensity of the Si peak compared with Mn and Fe peaks indicates that the $MnFe_2O_4$

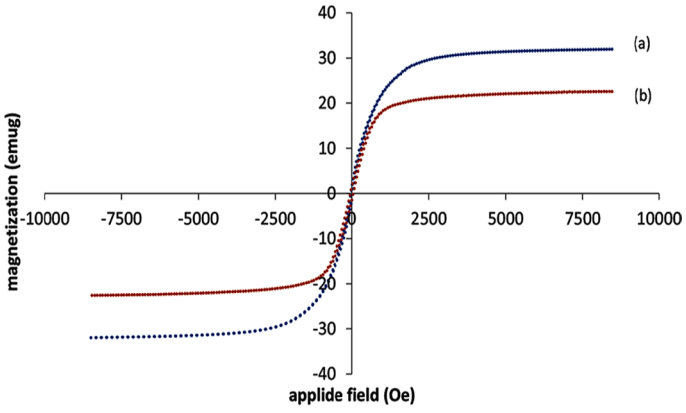

Fig. 4 VSM analysis for **a** $MnFe_2O_4$ and **b** MNPs@SiO_2-BTEAT-SO_3H

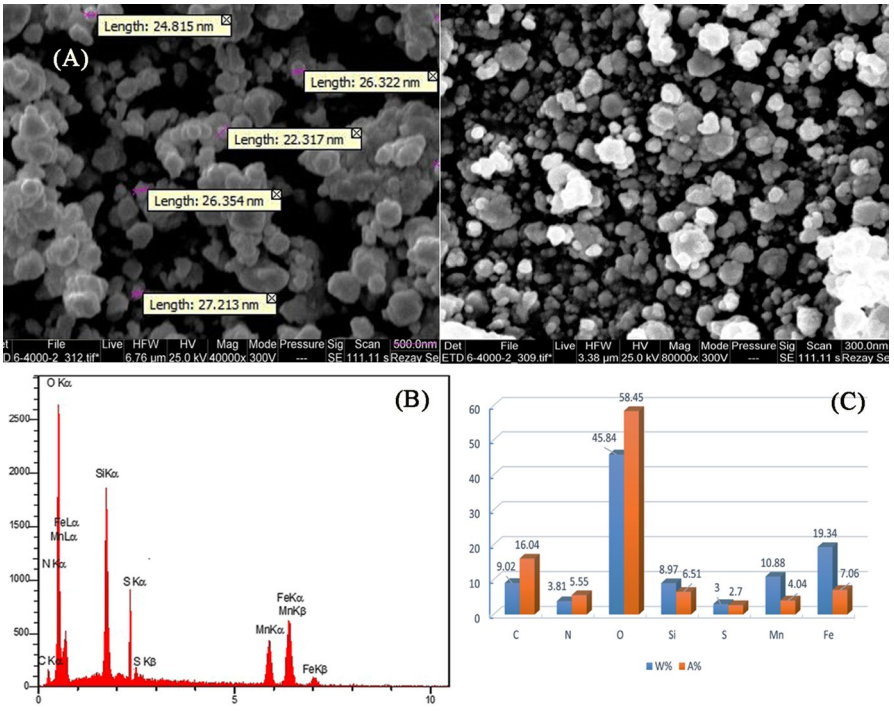

Fig. 5 FE-SEM (**a**), EDS (**b**) and column chart for quantitative results obtained from EDS (**c**) analyses for MNPs@SiO_2-BTEAT-SO_3H

nanoparticles were coated by SiO_2 shell. Also, besides the column chart for quantitative results obtained from EDS analysis is shown in Fig. 5c. Based on the column chart, W% for S/N is 0.70 that is in agreement with the proposed structure of nanoparticles (S/N = 0.66). EDS map scanning spectra in Fig. 6 show the dispersion–aggregation phenomenon of Si, O, C, N, S, Fe, Mn and integration of the outer surface of MNPs@SiO_2-BTEAT-SO_3H particles. The different color spots over the dark background confirm the location of the relative elements on the external surface of MNPs@SiO_2-BTEAT-SO_3H particles. The blue, purple, red, white, orange, golden, green and integration spots in Fig. 6 corresponded to carbon (C), iron (Fe), manganese (Mn), nitrogen (N), sulfur (S), oxygen (O), silicon (Si) and integration, respectively.

The catalytic activity of MNPs@SiO_2-BTEAT-SO_3H

The catalytic activity of MNPs@SiO_2-BTEAT-SO_3H was carefully investigated in the synthesis of spiroperimidines, pyranopyrazoles and spiropyranopyrazoles (Schemes 2, 3). Primitively, the catalytic activity of MNPs@SiO_2-BTEAT-SO_3H was examined in the synthesis of spiroperimidine derivatives. The reaction of cyclohexanone (1 mmol) and naphthalene-1,8-diamine (1 mmol) as a

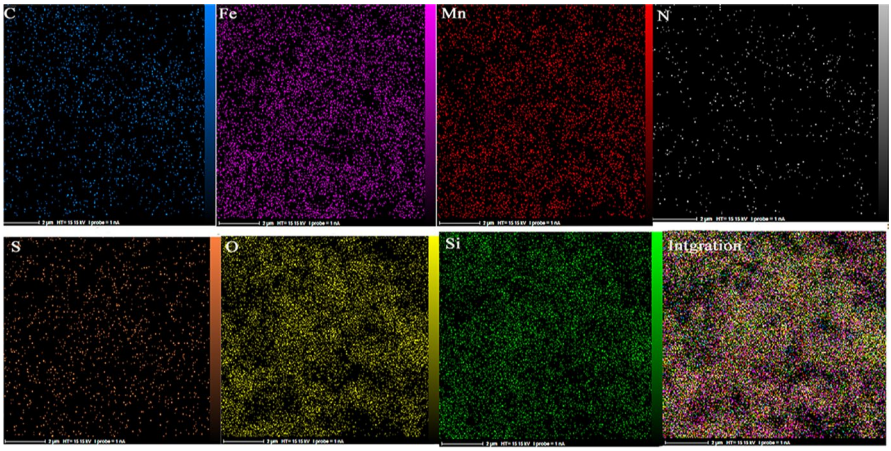

Fig. 6 EDS map analysis for MNPs@SiO_2-BTEAT-SO_3H

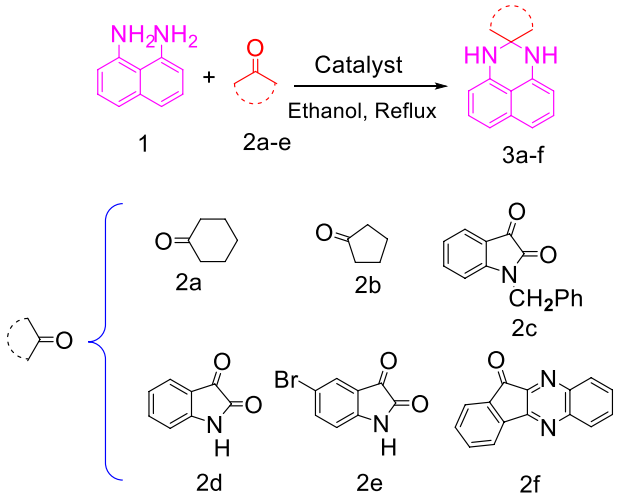

Scheme 2 Synthetic pathway of spiroperimidine derivatives

model reaction was performed in various conditions (Table 1). The results show the most productive efficiency gained in the presence of 20 mg MNPs@SiO_2-BTEAT-SO_3H as a catalyst and EtOH/H_2O as solvent at reflux condition (Table1, Entry 6). Also, the presence of a catalyst is necessary for reaction performance (Table1, Entry 5). Finally, the model reaction was performed in the presence of other MNPs ($MnFe_2O_4$, $MnFe_2O_4$@SiO_2, $MnFe_2O_4$@SiO_2-$PrNH_2$, $MnFe_2O_4$@SiO_2-Pr-$TDCl_2$ and $MnFe_2O_4$@SiO_2-Pr-BTEAT) as catalysts and the results are shown in Table 1 (Entries 9–13). After optimizing the conditions, the synthesis of spiroperimidine derivatives was carried out and high yields (73–94%) of the desired products obtained (Scheme 2, Table 2). All the products were carefully

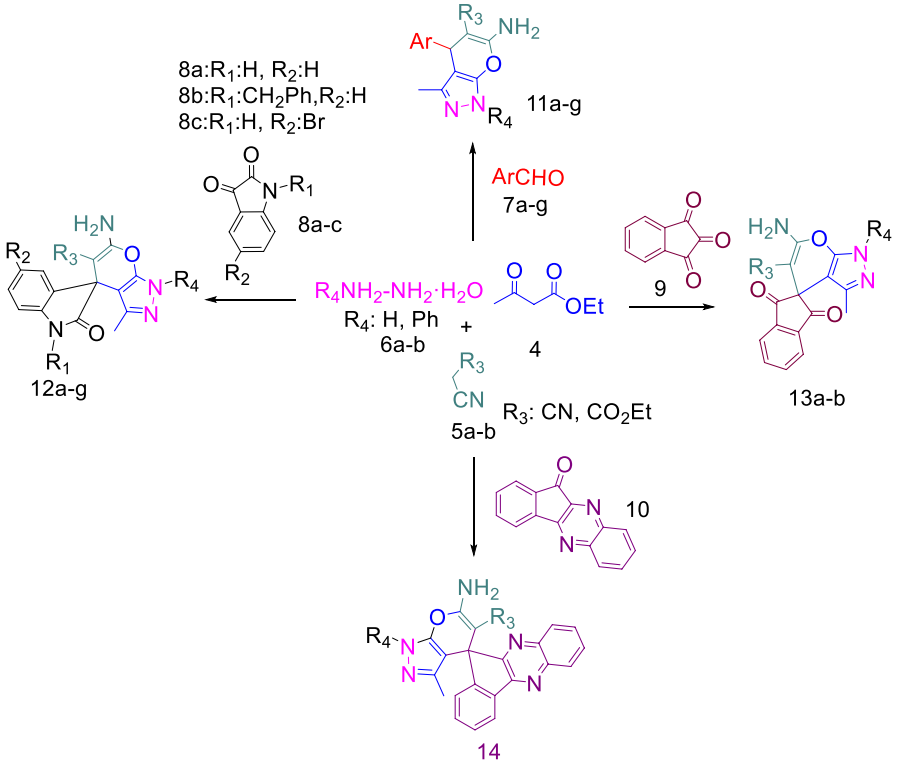

Scheme 3 Synthetic pathway of spiropyranopyrazoles and pyranopyrazoles

characterized by possible comparison of physical constants, elemental analysis, FT-IR, ^{1}H-NMR and ^{13}C-NMR spectroscopy (**SI**). In continuation, this work was compared with other reported procedures for the synthesis of spiroperimidine derivatives (Table 3). The results confirm MNPs@SiO_2-BTEAT-SO_3H is a suitable and efficient catalyst in the synthesis of spiroperimidines with respect to time and yield.

At the second step, the catalytic activity of MNPs@SiO_2-BTEAT-SO_3H was studied in the model reaction of 4-chlorobenzaldehyde, malononitrile, ethyl acetoacetate and hydrazine hydrate to afford the desired pyranopyrazole product (Table 4). The reaction was performed in the presence of varying amounts of catalyst, various solvents and different temperatures (Table 4). The results show the best efficiency gained in the presence of 15 mg MNPs@SiO_2-BTEAT-SO_3H as a catalyst and H_2O as solvent at room temperature (Table 4, Entry 4). Moreover, the presence of a catalyst is necessary for reaction performance, and the catalytic activity of MNPs@SiO_2-BTEAT-SO_3H is superior in comparison with other catalysts (Table 4, Entries 2, 8–12).

After optimizing the reaction, various carbonyl compounds were used in the reaction and the desired products were obtained in high yields within short times

Table 1 Optimization for the synthesis of spiroperimidine derivatives in the presence of model reaction

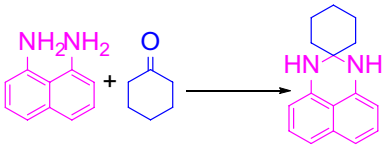

Entry	Conditions/solvent	Catalyst	Time (h)	Yield[a] (%)
1	Reflux/H_2O	MNPs@SiO_2-BTEAT-SO_3H (10 mg)	4	75
2	Reflux/EtOH	MNPs@SiO_2-BTEAT-SO_3H (10 mg)	1.45	80
3	Reflux/EtOH:H_2O (1:1)	MNPs@SiO_2-BTEAT-SO_3H (10 mg)	2.30	75
4	80 °C/Solvent-free	MNPs@SiO_2-BTEAT-SO_3H (10 mg)	2	80
5	Reflux/EtOH	–	24	Trace
6	70 °C/EtOH	MNPs@SiO_2-BTEAT-SO_3H (20 mg)	1	94
7	70 °C/EtOH	MNPs@SiO_2-BTEAT-SO_3H (30 mg)	1	93
8	r.t/EtOH	MNPs@SiO_2-BTEAT-SO_3H (20 mg)	7	40
9	70 °C/EtOH	$MnFe_2O_4$ (20 mg)	1	79
10	70 °C/EtOH	$MnFe_2O_4$@SiO_2(20 mg)	1	57
11	70 °C/EtOH	$MnFe_2O_4$@SiO_2-$PrNH_2$ (20 mg)	1	75
12	70 °C/EtOH	$MnFe_2O_4$@SiO_2-Pr-$TDCl_2$(20 mg)	1	67
13	70 °C/EtOH	$MnFe_2O_4$@SiO_2-BTEAT(20 mg)	1	80

[a]Isolated yield

Table 2 Synthesis of spiroperimidine derivatives in the presence of MNPs@SiO_2-BTEAT-SO_3H (20 mg) nanoparticles as catalyst

Entry	Compounds	Product	Time (h)	Yield (%)[a]	mp (°C)	
					Obtained	Reported
1	2a	**3a**	1	94	109–110	110–111 [27]
2	2b	**3b**	3	73	85–88	84–86 [18]
3	2c	**3c**	1.5	85	171–172	171–173 [27]
4	2d	**3d**	1	87	240–241	242–244 [18]
5	2e	**3e**	2	80	230–233	236 [33]
6	2f	**3f**	2	92	282–283	> 290 [33]

[a]Isolated yield, reaction conditions: naphthalene-1,8-diamine (**1**, 1 mmol, 0.2 g), ketone (**2a–b**)/isatin derivatives (**2c–e**)/1*H*-indeno[1,2-*b*] quinoxalin-11-one (**2f**, 1 mmol) and MNPs@SiO_2-BTEAT-SO_3H (20 mg) in the presence of 5 mL ethanol at 70 °C

(Scheme 3, Table 5). Initially, various aromatic aldehydes were used as starting carbonyl compounds and the equivalent products were produced in excellent yields (Table 5, Entries 1–7). The presented results confirm that the reactions with aromatic aldehydes bearing electron-withdrawing substituents are

Table 3 Comparison of MNPs@SiO_2-BTEAT-SO_3H catalyst with other reported catalysts in the synthesis of spiroperimidine in model reaction[a]

Entry	Condition	Catalyst	Time (min)	Yield (%)	References
1	H_2O: EtOH, 50 °C	MNPs-TBSA	120	70	[27]
2	EtOH, 75 °C	Phenylboronic acid	30	92	[34]
3	Solvent-free, 70 °C	SA	75	81	[33]
4	EtOH, 70 °C	MNPs@SiO_2-BTEAT-SO_3H	60	94	This work

[a]Reagents: 1,8-diaminonaphtalene (1 mmol), cyclohexanone (1 mmol)

Table 4 Optimization of the reaction conditions for the synthesis of pyranopyrazole derivatives in the presence of model reaction

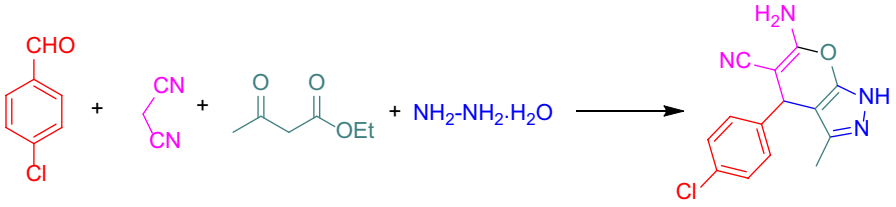

Entry	Conditions/solvent	Catalyst (mg)	Time (min)	Yield (%)[a]
1	r.t/H_2O	MNPs@SiO_2-BTEAT-SO_3H (10 mg)	30	87
2	r.t/H_2O	–	420	25
3	r.t/H_2O	MNPs@SiO_2-BTEAT-SO_3H (15 mg)	15	95
4	r.t/H_2O	MNPs@SiO_2-BTEAT-SO_3H (30 mg)	15	93
5	r.t/EtOH	MNPs@SiO_2-BTEAT-SO_3H (15 mg)	35	75
6	r.t/EtOH:H_2O (1:1)	MNPs@SiO_2-BTEAT-SO_3H (15 mg)	30	75
7	H_2O/reflux	MNPs@SiO_2-BTEAT-SO_3H (15 mg)	25	83
8	r.t/H_2O	$MnFe_2O_4$ (15 mg)	30	77
9	r.t/H_2O	$MnFe_2O_4$@SiO_2 (15 mg)	45	65
10	r.t/H_2O	$MnFe_2O_4$@SiO_2-PrNH_2 (15 mg)	40	73
11	r.t/H_2O	$MnFe_2O_4$@SiO_2-Pr-$TDCl_2$ (15 mg)	50	67
12	r.t/H_2O	$MnFe_2O_4$@SiO_2-NH-BTEAT (15 mg)	35	73

[a]Isolated yield

performed in shorter times than aldehydes including electron-donating substituents. At the second step, various ketones including indoline-2,3-dione derivatives, 1*H*-indene-1,2,3-trione and 11*H*-indeno[1,2-*b*]quinoxalin-11-one were inserted in the designed reaction and the desired valuable spiroproducts were acquired in good yields (Table 5, Entries 8–17). To the best of our knowledge, the product **11g**, **13a** and **14** are synthesized for the first time. All the products were carefully characterized by possible comparison of physical constants, elemental analysis,

Table 5 Synthesis of pyranopyrazole and spiropyranopyrazole derivatives in the presence of MNPs@SiO_2-BTEAT-SO_3H as a catalyst

Entry	Ar or carbonyl compound	R_4	R_3	Product	Time (min)	Yield (%)	Mp (°C)	
							Obtained	Reported
1	4-Cl–C_6H_4	H	CN	**11a**	15	95	230–232	226–228 [35]
2	2,4-$(Cl)_2$–C_6H_3	H	CN	**11b**	20	92	231–232	229–230 [36]
3	4-OMe–C_6H_4	H	CN	**11c**	30	87	206–208	210–212 [37]
4	4-Me–C_6H_4	H	CN	**11d**	25	80	200–202	208–209 [38]
5	4-Br–C_6H_4	H	CN	**11e**	45	80	180–181	183–185 [39]
6	4-Cl–C_6H_4	Ph	CN	**11f**	115	81	218–220	203–205 [40]
7	3-NO_2–4-OH–C_6H_3	H	CN	**11g**	35	95	223	–
8	8a	H	CN	**12a**	100	95	285–287	278–280 [25]
9	8b	H	CN	**12b**	80	93	255–257	268–270 [25]
10	8c	H	CN	**12c**	110	85	280–283	281 [25]
11	8a	H	CO_2Et	**12d**	140	80	280–281	280–282 [25]
12	8b	H	CO_2Et	**12e**	125	85	127–130	126–127 [41]
13	8c	H	CO_2Et	**12f**	145	78	255–256	250–254 [39]
14	9	H	CN	**13a**	100	83	291–292	–
15	10	Ph	CN	**14**	200	80	248–249	–
16	8a	Ph	CN	**12g**	130	82	225–226	227–229 [41]
17	9	Ph	CN	**13b**	180	81	219–220	220–222 [40]

[a]Isolated yield, Reaction conditions: aryl aldehydes (1 mmol) or ketones (1 mmol), hydrazine hydrate (1.5 mmol), ethyl acetoacetate (1 mmol), malononitrile (1 mmol) and MNPs@SiO_2-BTEAT-SO_3H (15 mg) in the presence of 10 mL water at room temperature

Table 6 Comparison of MNPs@SiO_2-BTEAT-SO_3H catalyst with other catalysts reported for the synthesis of spiropyranopyrazoles in the model reaction[a]

Entry	Condition	Catalyst	Time (min)	Yield (%)	References
1	H_2O, 80 °C	Nano-SiO_2	35	90	[37]
2	Solvent-free, 90 °C	[DMBSI]HSO4	18	88	[42]
3	Solvent-free, 100 °C	Nano[Fe-PSMP]Cl_2	5	85	[43]
4	EtOH:H_2O, 60 °C	Aspirin	30	92	[39]
5	H_2O, r.t	Meglumine	15	95	[36]
6	H_2O, r.t	($NiFe_2O_4$@SiO_2-Preyssler) NFS-PRS	15	97	[29]
7	H_2O:EtOH (9:1), 80 °C	β-Cyclodextrin	15	92	[44]
8	Solvent-free, 100 °C	[cmpy]I	4	94	[35]
9	H_2O, r.t	MNPs@SiO_2-BTEAT-SO_3H	15	95	This work

[a]Reagents: malononitrile (1 mmol), hydrazinhydrate (1 mmol), 4-chlorobenzaldehyde (1 mmol), ethylacetoacetate (1 mmol)

FT-IR, ^{1}H-NMR and ^{13}C-NMR spectroscopy (**SI**). The comparison of MNPs@SiO_2-BTEAT-SO_3H catalyst with other reported catalysts in the model reaction is provided in Table 6. The MNPs@SiO_2-BTEAT-SO_3H displays good or higher performance in comparison with other catalysts.

Reusability of recyclability the MNPs@SiO_2-BTEAT-SO_3H catalyst

In the green synthetic processes, the reusability and recyclability of catalysts are essential. Therefore, the reusability of MNPs@SiO_2-BTEAT-SO_3H was evaluated in the model reactions. After completion, the solvent was evaporated, the precipitate was dissolved in ethanol and the catalyst was separated by a magnet. The recovered catalyst was reused in the ensuing reaction without further activation. As shown in Fig. 7a, the catalyst could be recycled without any change in catalytic activity in five runs. The FT-IR spectra (Fig. 7b) and XRD patterns (Fig. 7c) of fresh and reused catalysts are compared. The reused catalyst receives no noticeable change in structure. Also, Fig. 7d indicates an easy separation of the hybrid catalyst by an external magnet (a) and re-dispersion of MNPs@SiO_2-BTEAT-SO_3H after removal of the magnet (b). These results confirm that the MNPs@SiO_2-BTEAT-SO_3H has excellent stability and performance in organic reactions.

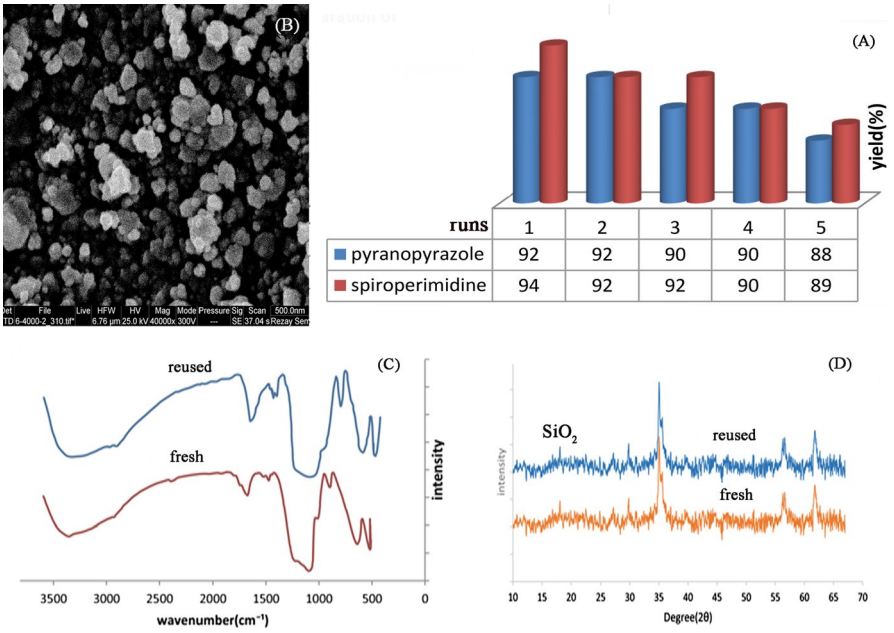

Fig. 7 Recyclability of MNPs@SiO_2-BTEAT-SO_3H (**a**), FT-IR spectra (**b**) and XRD patterns (**c**) of the reused and fresh catalyst, magnetic separation and re-dispersion of catalyst (**d**)

Plausible mechanism for the synthesis of products in the presence of MNPs@SiO_2-BTEAT-SO_3H as a catalyst

A plausible pathway for the synthesis of spiroperimidine derivatives in the presence of the MNPs@SiO_2-BTEAT-SO_3H catalyst is shown in Scheme 4. Initially, the carbonyl group is typically activated by MNPs@SiO_2-BTEAT-SO_3H catalyst, and a nucleophilic attack of the 1,8-diaminonaphthalene on the activated carbonyl group produces intermediate A. The imine bond attacked by NH_2, and intermediate B performed. At last, the possible removal of H^+ afforded the desired spiroperimidine [27].

A proposed mechanism for the synthesis of pyranopyrazole derivatives in the presence of MNPs@SiO_2-BTEAT-SO_3H is described in Scheme 5. Initially, a condensation of hydrazine hydrate and ethyl acetoacetate produces the 3-methyl-1*H*-pyrazol-5-ol (intermediate A). The Knoevenagel condensation between malononitrile and activated carbonyl compound produced the arylidenemalononitrile (intermediate B). Subsequently, the Michael addition takes place between intermediate A and intermediate B and the successive tautomerization resulted in the pyranopyrazole formation [25, 45]. For consolidation, the intermediates A and B were synthesized and identified (SI). The typical reaction of as-prepared intermediates A and B successfully produced the desired product.

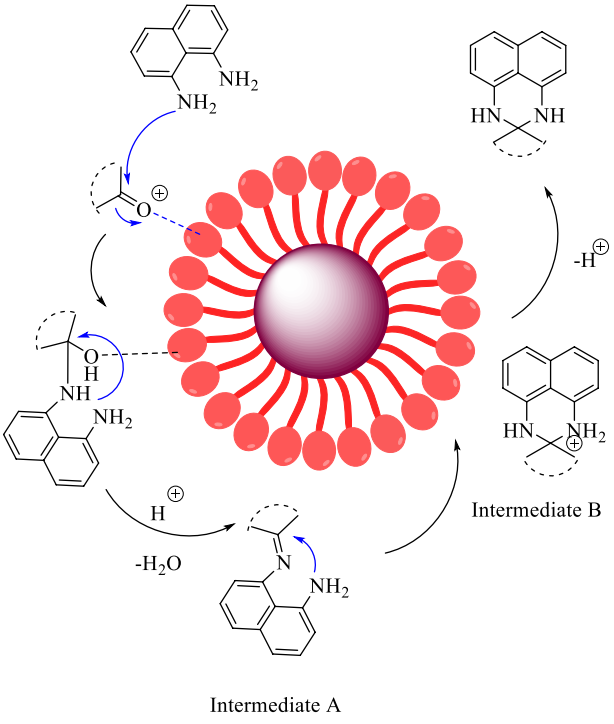

Scheme 4 Plausible mechanism for the synthesis of spiroperimidines

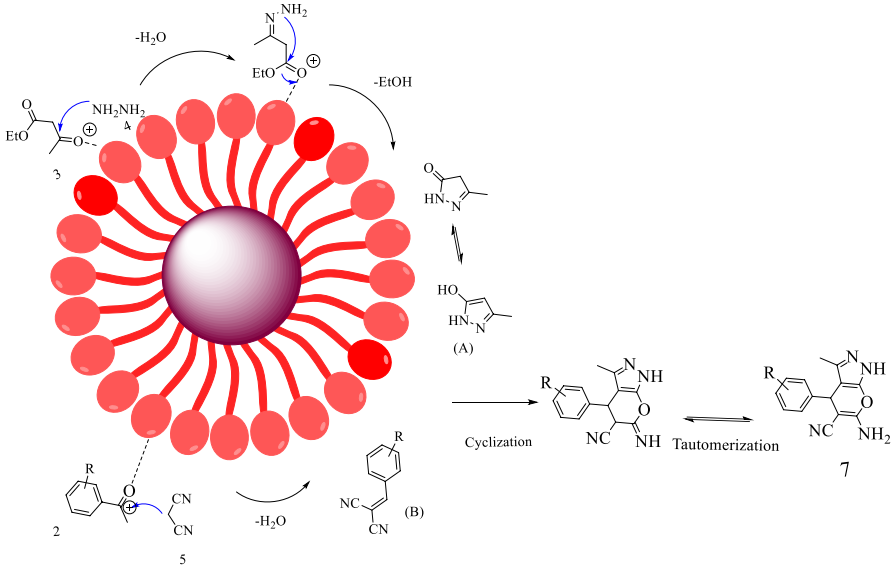

Scheme 5 The plausible mechanism for the synthesis of pyranopyrazoles

Conclusion

A new hybrid inorganic–organic nanocatalyst (MNPs@SiO_2-BTEAT-SO_3H) as a recyclable and highly efficient heterogeneous catalyst was prepared. The FT-IR, XRD, VSM, EDS, EDS map and SEM analysis techniques have been confirmed the successful preparation of hybrid nanostructure and its excellent stability. The application of MNPs@SiO_2-BTEAT-SO_3H in the organic synthesis confirms its efficiency as a suitable heterogeneous catalyst in the synthesis of spiroperimidines, pyranopyrazole and spiropyranopyrazole derivatives. The MNPs@SiO_2-BTEAT-SO_3H has high acidity. In addition, we think that the long organic tags grafting and triazine ring moiety resulted in an intense performance of MNPs@SiO_2-BTEAT-SO_3H in organic solvents and aqueous medium. The advantages of this work are high yields, short reaction times, use of a green solvent, easy workup procedure, catalyst reusability without significant diminishing in its efficiency and simple separation of hybrid nanocatalyst by applying an external magnet.

Acknowledgements This study was supported by the Research Council of Arak University (Grant No. 94Ah.Ph.D).

Compliance with ethical standards

Conflict of interest The authors have no other conflict of interest to declare.

References

1. K. Li, Y. Fan, Y. He, L. Zeng, X. Han, Y. Yan, Sci. Rep. **7**, 1 (2017)
2. A.A. Alqadami, M. Naushad, Z.A. Alothman, A.A. Ghfar, Appl. Mater. **9**, 36026 (2017)
3. A.A. Alqadami, M. Naushad, M.A. Abdalla, T. Ahamad, Z.A. Alothman, S.M. Alshehri, A.A. Ghfar, J. Clean. Prod. **156**, 426 (2017)
4. Z. Rashid, H. Naeimi, A.-H. Zarnani, M. Nazari, M.-R. Nejadmoghaddam, R. Ghahremanzadeh, RSC Adv. **6**, 36840 (2016)
5. D. Wang, D. Astruc, Chem. Rev. **114**, 6949 (2014)
6. M.A. Bodaghifard, M. Hamidinasab, N. Ahadi, Curr. Org. Chem. **22**, 234 (2018)
7. H. Tombuloglu, G. Tombuloglu, Y. Slimani, I. Ercan, H. Sozeri, A. Baykal, Environ. Pollut. **243**, 872 (2018)
8. T. Kang, F. Li, S. Baik, W. Shao, D. Ling, T. Hyeon, Biomaterials **136**, 98 (2017)
9. M. Jacintha, P. Neeraja, M. Sivakumar, K. Chinnaraj, J. Supercond. Novel. Magn. **30**, 237 (2017)
10. F. Bonyasi, M. Hekmati, H. Veisi, J. Colloid, Interface Sci. **496**, 177 (2017)
11. A.K. Rathi, R. Zboril, R.S. Varma, M.B. Gawande, *Ferrites and Ferrates: Chemistry and Applications in Sustainable Energy and Environmental Remediation* (ACS Publications, Washington, 2016), pp. 39–78
12. F. Chen, J. Zheng, M. Huang, Y. Li, Res. Chem. Intermed. **41**, 5545 (2015)
13. H. Sachdeva, S. Khaturia, MOJ. Biorg. Org. Chem. **1**, 239 (2017)
14. P.N. Sudhan, M. Ghashang, S.S. Mansoor, Beni Seuf. Univ. J. Appl. ScI. **5**, 340 (2016)
15. F. Behbahani, F.M. Golchin, J. Taibah. Univ. Sci. **11**, 85 (2017)
16. R. Kumar, N. Yadav, R. Lavilla, D. Blasi, J. Quintana, J.M. Brea, M.I. Loza, J. Mestres, M. Bhandari, R. Arora, Mol. Divers. **21**, 533 (2017)
17. A. Moshtaghi Zonouz, D. Moghani, Synth. Commun. **46**, 220 (2016)
18. V.V. Patil, G.S. Shankarling, Catal. Commun. **57**, 138 (2014)
19. N.A. Harry, R.M. Cherian, S. Radhika, G. Anilkumar, Tetrahedron Lett. **60**, 150946 (2019)
20. B.B.F. Mirjalili, M. Imani, J. Chin. Chem. Soc Taip. **66**, 1542 (2019)
21. Q. Niu, J. Xi, L. Li, L. Li, C. Pan, M. Lan, L. Rong, Tetrahedron Lett. **60**, 151181 (2019)
22. Z. Wang, L. Gao, Z. Xu, Z. Ling, Y. Qin, L. Rong, S.-J. Tu, Tetrahedron **73**, 385 (2017)
23. H. Naeimi, S. Lahouti, RSC Adv. **7**, 2555 (2017)
24. B. Maleki, N. Nasiri, R. Tayebee, A. Khojastehnezhad, H.A. Akhlaghi, RSC Adv. **6**, 79128 (2016)
25. G.M. Ziarani, M. Rahimifard, F. Nouri, A. Badiei, J. Serb. Chem. Soc. **80**, 1265 (2015)
26. M. Abdi, S. Rostamizadeh, N. Zekri, Polycycl. Aromat. Compd. **39**, 413 (2019)
27. M.A. Bodaghifard, S. Asadbegi, Z. Bahrami, J. Iran. Chem. Soc. **14**, 365 (2017)
28. H. Kefayati, S.J. Bazargard, P. Vejdansefat, S. Shariati, A.M. Kohankar, Dyes Pigm. **125**, 309 (2016)
29. A. Javid, A. Khojastehnezhad, H. Eshghi, F. Moeinpour, F.F. Bamoharram, J. Ebrahimi, Org. Prep. Proced. Int. **48**, 377 (2016)
30. N. Ahadi, M.A. Bodaghifard, A. Mobinikhaledi, Appl. Organomet. Chem. **33**, e4738 (2019)
31. J.-Q. Zhu, X.-J. Zhang, S.-W. Wang, G.-S. Wang, P.-G. Yin, RSC Adv. **6**, 88104 (2016)
32. J. Li, H. Zhao, X. Hou, W. Fa, J. Cai, Micro. Nano Lett. **12**, 53 (2017)
33. M.A. Bodaghifard, N. Ahadi, Iran. J. Catal. **6**, 377 (2016)
34. V.D. Patil, K.P. Patil, N.R. Sutar, P.V. Gidh, Chem. Int. **3**, 195 (2017)
35. A.R. Moosavi-Zare, M.A. Zolfigol, R. Salehi-Moratab, E. Noroozizadeh, J. Mol. Catal. A. Chem. **415**, 144 (2016)
36. R.-Y. Guo, Z.-M. An, L.-P. Mo, S.-T. Yang, H.-X. Liu, S.-X. Wang, Z.-H. Zhang, Tetrahedron **69**, 9931 (2013)
37. K.G. Patel, N.M. Misra, R.H. Vekariya, R.R. Shettigar, Res. Chem. Intermed. **44**, 289 (2018)
38. A.S. Waghmare, S.S. Pandit, D.M. Suryawanshi, Comb. Chem. High. Throughput Screen. **21**, 254 (2018)
39. M. Fatahpour, F.N. Sadeh, N. Hazeri, M.T. Maghsoodlou, M. Lashkari, J. Iran. Chem. Soc. **14**, 1945 (2017)
40. T. Liu, C.B. Li, Y.Q. Yu, D.Z. Xu, ChemistrySelect **2**, 2917 (2017)
41. S.F. Hojati, A. Amiri, S. Mohamadi, N. MoeiniEghbali, Res. Chem. Intermed. **44**, 2275 (2018)

42. P. Farokhian, M. Mamaghani, N.O. Mahmoodi, K. Tabatabaeian, J. Iran. Chem. Soc. **15**, 11 (2018)
43. A.R. Moosavi-Zare, H. Goudarziafshar, K. Saki, Appl. Organomet. Chem. **32**, e3968 (2018)
44. Y.A. Tayade, S.A. Padvi, Y.B. Wagh, D.S. Dalal, Tetrahedron Lett. **56**, 2441 (2015)
45. A. Upadhyay, L.K. Sharma, V.K. Singh, R. Dubey, N. Kumar, R.K.P. Singh, Tetrahedron Lett. **58**, 1245 (2017)